M_L scale in Northwestern Turkey from 1999 Izmit aftershocks: updates

D. Bindi[2], S. Parolai[1], E. Görgün[1], H. Grosser[1], C. Milkereit[1], M. Bohnhoff[1], E. Durukal[3]

[1] GeoForschungsZentrum Potsdam, Telegrafenberg, 14473 Potsdam, Germany.
[2] Istituto Nazionale di Geofisica e Vulcanologia, via Bassini 15, 20133 Milano, Italy.
[3] Bogazici University, Department of Earthquake Engineering, Istanbul, Turkey

Abstract.

We present an update of the local magnitude scale previously calibrated for Northwestern Turkey by Baumbach et al. (2003). The path coverage in the westernmost part of the analysed area has been increased, as well as the number of amplitudes for distance greater than 110 km. Furthermore, a set of recordings from accelerometric stations operated by the Kandilli Observatory and Earthquake Research Institute (KOERI) has been merged with the recordings by the Sapanca-Bolu and GermanTaskForce seismological networks. In all, 4047 recordings from 528 earthquakes recorded by 31 seismometers and 23 accelerometers are considered to calibrate the local magnitude scale over a hypocentral distance range from 10 to 190 km. By analyzing the unit covariance matrix and the resolution matrix, we show how the source-to-station geometries of the seismic and strong motion networks affect the uncertainties of the computed station corrections, attenuation coefficients, and magnitudes. The assumptions made concerning the reference station correction, and the change in the amplification for the Wood-Anderson torsion seismograph from 2800 to 2080 (Uhrhammer and Collins, 1990) introduced an offset of about 0.34 in the magnitudes with respect to Baumbach et al. (2003), with the updated local magnitude scale ranges from 0.50 to 5.91. The distribution of the residuals with distance confirms that the extension of both the magnitude and distance ranges and the improved path coverage have preserved the high quality that characterized the data set analyzed by Baumbach et al. (2003).

Introduction

Within the framework of the Megacity project Istanbul (http://www.cedim.de, working program link), new attenuation relationships for northwestern Turkey have to be derived. This requires a well-constrained magnitude scale that can be applied to a data set including not only the earthquakes recorded by the seismic networks deployed in Northwestern Turkey but also strong motion data. With this aim, in this work we update the local magnitude scale previously calibrated for Northwestern Turkey by Baumbach et al. (2003), hereinafter referred to as B03. The main improvements to results from B03 are an enlarged data base (in term of areal coverage and magnitude range) and improvements with regards to the inversion procedure. Furthermore, even if not considered in the location procedure, recordings form 23 accelerometers operated by the Kandilli Observatory and Earthquake Research Institute (KOERI) are also considered for calibrating the magnitude scale.

The distribution of the earthquakes we selected allows the improvement of the path coverage in the westernmost part of the analysed area and to increase the sampling of the portion of the path greater than 110 km. We performed the inversion to calibrate the magnitude scale applying some constraints that are different from those applied by B03. Following an earlier study on site amplification effects (Parolai et al., 2004), we assume station 39 (Figure 1), which is installed on rock, as reference station for the Sapanca-Bolu (SABO) and German Task Force (GTF) seismic networks. Its magnitude station correction is set to zero, while in B03 the average station correction of the whole network was constrained to zero. This work is organized as follows: first, we describe the data set used to calibrate the magnitude scale and discuss the covariance and resolution matrices. Then, we calibrate the magnitude scale by computing the magnitude station corrections and the attenuation with distance coefficients. Finally, we compare our results with those from B03

.

Data

We calibrated a local magnitude scale using recordings of the 1999 Izmit aftershocks from both seismic (GTF and SABO) and strong motion (KOERI) networks. From the seismic stations belonging to the SABO network and to the temporary GTF network (B03), 3871 recordings of 490 earthquakes that occurred between August 22 and October 16, 1999 have been considered. The hypocentres have been computed using a standard location procedure (Klein, 2002) that considered the arrival times at stations of the GTF and SABO networks. We also considered 176 accelerograms from 48 earthquakes that occurred between August 21 and December 12, 1999 and recorded by the KOERI accelerometric network ((http://koeri.bound.edu.tr). For these earthquakes, except for 10 that were also recorded by the SABO and GTF networks, we used the locations provided by the KOERI. In total, the magnitude scale has been calibrated by considering 4047 recordings relevant to 528 earthquakes and recorded by 31 seismometers and 23 accelerometers (Table 1).

Figure 1 shows the source-to-station path coverage, over the distance range 10 to 190 km. With respect to the data set previously analysed by B03 (their Figure 1), the path coverage has been increased, especially in the westernmost part of the analyzed region, toward the Bay of Izmit. Moreover, the number of recordings having an hypocentral distance larger than 110 km has been increased from 105 to 178.

Figures 2 and 3 show the resolution and the unit covariance matrices (Menke, 1984), computed for the design matrix relative to the standard non parametric functional for local magnitude calibration (e.g., Richter 1935; Savage and Anderson, 1995)

$$\log A(R) = Ml + \log A_o(R_i) + S \qquad (1)$$

where A is the measured maximum horizontal amplitude in millimetres read from the synthesized Wood-Anderson seismogram, R is the hypocentral distance, $\log A_o$ is the distance-dependent attenuation curve and S is a station-dependent magnitude adjustment factor. The distance range from 10 to 190 km has been discretized into 60 segments of 3 km width. In equation (1), R_i

represents the knots of the discretization and $R_i \leq R < R_{i+1}$. We add several constraints to equation (1). The first, the $logA_o$ function is constrained to assume the value -2 at 17 km (Hutton and Boore, 1987) and to be a smooth function with distance, by constraining the second derivative to be small. To avoid the trade-off between station corrections and magnitudes, a constraint is also applied to S. In particular, we add two rows to the linear system derived from (1): in the first, we constrain *S* for station 39 (i.e., the reference station) to be zero while, in the second row, we require that the station corrections for the KOERI accelerometer network sum to zero, since a reference station is not available for the accelerometer network. The applied constraints to S mean that we assume a reference station for the SABO and GTF networks, as Parolai et al. (2004) did when determining the site amplification effects, whereas the reference for the KOERI network is the network average station correction. We considered station 39 as the reference because it is a permanent station installed on rock and it shows an almost flat site transfer function (Parolai et al., 2004). Moreover, it is the station having the second highest number of recordings in our data set (Table 1), and the back-azimuth of the earthquakes covers a wide range (about 180^o). We performed a test by constraining to zero the average correction of stations 39 and 02. The latter is also a station installed on rock that recorded a large number of earthquakes and it is located far from station 39 (Figure 1). The calibrated magnitude scale (here not shown) was very similar to that obtained constraining to zero the correction of station 39 alone. Considering that, differently form station 02, station 39 is a permanent station that can be used as a reference also for future earthquake recordings in Northwestern Turkey, we will show and discuss only the scale calibrated using only station 39 as reference.

The resolution and covariance matrices have been computed via a singular value decomposition of the design matrix (Press et al., 1992). The regularization needed to treat the ill-conditioned nature of the inverse problem has been performed cutting the singular values less than 0.01 times the maximum singular value. Figure 2 shows that the resolution matrix is almost diagonal, suggesting that the source-to-station geometry, the performed discretization and the applied constraints allow

us to resolve satisfactorily the unknowns. Only a weak trade-off exists between the station corrections and the attenuation with distance coefficients, especially for distances <40 km, that correspond to columns of the design matrix <11. Hereinafter we refer to each column of the design matrix as parameter index (PI). For these distances, a weak smearing between the coefficients of neighbour knots is also present.

The unit covariance matrix shown in Figure 3 provides an image of the amplification of errors from the data to the solutions. The diagonal elements of the unit covariance matrix are also shown in Figure 4. For the attenuation coefficients (PI ≤ 61), the amplification factor for the variance (region (a) in Figure 4) are smaller than 0.2, and the increase with distance of the importance of the cross-errors propagating from adjacent intervals (off-diagonal elements) reflects the diminishment of the number of recordings with distance. The propagation of errors for the magnitude values can be split into two parts: for parameter index between 62 and 551, about 88% of the amplification factors for the variance are less than 0.5 (region (b) in Figure 4), and the cross-propagation of errors between different earthquakes is negligible. In contrast, for PI between 552 and 589 (region (c) in Figure 4) the cross-propagation of error is significant (about 50% larger than 0.5). The magnitudes in this parameter index range are relevant to earthquakes recorded by the KOERI network. Similar considerations can be drawn for the station corrections (PI > 589): while the propagation of error for the SABO and GTF station corrections (590≤ PI ≤620) is weak (region (d) in Figure 4), high propagation factors for the KOERI network are observed (region (e) in Figure 4). It is worth noting that the resolution and unit covariance matrices only depend upon the coefficient matrices of equation (1), that is the quality of the data does not affect these matrices. Therefore, starting from accelerometric and velocimetric data of comparable quality, we expect that the station corrections for the KOERI network and the magnitude of earthquakes only recorded by accelerometers will be affected by higher uncertainties than the results for GTF and SABO networks. This difference in the stability of the results is due to the different source-to-station geometry of the seismological and strong motion networks, and to the weak cross-information between them.

Local magnitude scale

Figure 5 shows the results of the magnitude-scale calibration. The uncertainties for the distance coefficients, magnitudes and station corrections have been estimated by inverting 200 bootstrap replications of the data set (Efron, 1979; B03). The $logA_o$ attenuation function (Figure 5, top panel) is characterized by a decrease in the attenuation rate for path longer than 30 km, in fair agreement with B03, even if the updated $logA_o$ is about 0.1 units of magnitude smaller for distances in the range 25-110 km. Furthermore, the computed attenuation function is affected by post-critical reflections from the crust-mantle boundary (Moho) for offsets of around 110 km, as described in B03. However, this feature is now better constrained by the improved sampling of distances >110 km. The standard deviation for $logA_o$ is less than 0.04 for distances up to 110 km, and less than 0.07 for longer paths.

The obtained station corrections are shown in Figure 5 (middle panel) and in Table 1. As expected from the analysis of the unit covariance matrix, the standard deviation of the station corrections for the accelerometer network is higher than that for the seismometers, where the former varies from 0.131 to 0.386, while the latter ranges between 0.025 and 0.074. The average station corrections of the GTF and SABO networks vary from -0.129 to 0.923 units of magnitude, confirming the importance of the role played by the local site effects (B03; Parolai et al., 2004). Table 1 also shows the station corrections found by B03. The average difference between theB03 and the station corrections of this study is 0.40±0.02. No particular behaviour for different group of stations (e.g. depending on the position) is observed, confirming that the choice of constraining only one rock station does not introduced any significant bias. This was confirmed also by tests performed considering more than one reference station.

Finally, the average magnitudes within one standard deviation are show in Figure 5 (bottom panel). The mode and the median standard deviations are 0.059 and 0.076, respectively. The earthquakes identified by values of the variable EventID greater than 490 are recorded only by accelerometers

and the standard deviation for these earthquakes is higher, in agreement with the properties of the unit covariance matrix previously shown.

Conclusions

An extended data-set containing records of the aftershocks of the 1999 Izmit earthquake have been used to update the local magnitude scale for north-western Turkey calibrated by B03. We consider not only the recordings from the SABO and GTF seismic network, but we also add recordings from the accelerometric network operated by KOERI. The results for the strong motion network are affected by higher uncertainties, determined both by the lower quality characteristics of the resolution and covariance matrices for KOERI recordings and by the higher uncertainties affecting the input data (e.g., locations). Despite the higher uncertainties, we retained the accelerometric recordings because the calibrated scale provides a link to the accelerometric database that can be exploited for future studies on attenuation relationships for strong ground motion parameters.

The attenuation with distance curve $logA_0$ and the station corrections have been used to re-compute the magnitudes for the selected earthquakes, evaluated as the average of the station magnitudes. Figure 6 shows the magnitude versus distance distribution (top panel) as well as the distribution of the standard deviation of the average magnitude with the number of available recordings (middle panel). The magnitudes range from 0.50 to 5.91, and the standard deviation of most of the earthquakes having at least 9 recordings is less than 0.1. In Figure 6 (bottom panel) the comparison between the magnitudes computed using the results from B03 (Ml_{B03}) and from this study ($Ml_{this\ study}$) is shown. The best fitting line in the least squares sense is $Ml_{B03} = (0.972 \pm 0.004)\ Ml_{thistudy}+(0.340 \pm 0.001)$. From equation (1), the offset of 0.34 can be ascribed to (1) the difference in the Wood Anderson magnification, since the change from 2800 to 2080 (Uhrhammer and Collins, 1990) led to an offset of 0.129, (2) the difference in the average station corrections for the SABO and GTF networks (that is, 0 in B03 and 0.298 in this study) and (3) the difference of 0.1 magnitude unit between the attenuation functions.

Finally, Figure 7 shows the magnitude residuals computed for both the B03 magnitude scale (attenuation function and station corrections) and the scale updated in the present study. The distribution of the residuals with distance confirms that the extension of both the magnitude and distance ranges, and the improved path coverage have been obtained while still preserving the high quality that characterized the data set analyzed by B03. Furthermore, the updated magnitude scale better describes the attenuation properties in the analyzed area for distances larger than 110 km.

Acknowledgements

We thank M. Baumbach, S. Karakisa, E. Günther, and S. Zünbül for their contribution to the present study. The authors express their gratitude to the Hannover Rückversicherung AG for their significant financial support of the field mission. K. Fleming kindly improved our English. The figures were generated using the Wessel and Smith (1991) software. Part of this work was conducted during visits by one author (D. B.) to the GeoForschungsZentrum (GFZ) in Potsdam, that were partially funded by the GFZ.

References

Baumbach, M., D. Bindi, H. Grosser, C. Milkereit, S. Parolai, R.J. Wang, S. Karakisa, S. Zünbül, and J. Zschau (2003). Calibration of an M_L scale in Northwestern Turkey from 1999 Izmit aftershocks, *Bull. Seism. Soc. Am.,* **93**, 5, 2289-2295.

Efron , B. (1979). Bootstrap methods, another look at the jackknife, *Ann. Stat.* 7, 1-26.

Hutton, L. K., and D. M. Boore (1987). The Ml scale in southern California, *Bull. Seism. Soc. Am.,* **77**, 6, 2074-2094.

Klein, F. W. (2002). User′s Guide to HYPOINVERSE-2000, a Fortran Program to Solve for Earthquake Locations and Magnitudes, Open-File Report 02–171, *U.S. Geological Survey,* 123 pp.

Menke, W. (1984) *Geophysical Data Analysis: Discrete Inverse Theory*. Academic Press, New York.

Parolai S., D. Bindi, M. Baumbach, H. Grosser, C. Milkereit, S. Karakisa, S. Zünbül (2004), Comparison of different site response estimation techniques using aftershocks of the 1999 Izmit earthquake, *Bull. Seism. Soc. Am.,* **94**, 3, 1096-1108.

Press, W.H., Teulkolsky, S.A., Vetterling, W.T. and Flannery, B.P. (1992) *Numerical Recipes in C: The Art of Scientific Computing*, University Press, Cambridge.

Richter, C. F. 1935. An instrumental earthquake magnitude scale. *Bull. Seism. Soc. Am.*, **25**, 1-32.

Savage, M. K., and J. G. Anderson (1995). A local magnitude scale for the Western Basin-Eastern Sierra Nevada from Synthetic Wood-Anderson seismograms. *Bull. Seism. Soc. Am.,* **85***,* 1236-1243.

Uhrhammer, R. A., and E. R. Collins (1990). Synthesis of Wood-Anderson seismograms from broadband digital records, *Bull. Seism. Soc. Am.,* **80**, 702-716.

Wessel, P., and W.H.F. Smith (1991). Free software helps map and display data, *Eos. Trans. AGU* **72** (41), 441, 445-446.

Table 1.

ID	latitude	longitude	S	std	Nr	S_{B03}	Network
01	41.0083	29.2747	0.565	0.034	62	0.10	GTF
02	40.9682	29.5021	-0.013	0.029	180	-0.54	GTF
03	41.1189	29.6532	0.791	0.032	154	0.46	GTF
04	40.9111	29.6510	0.297	0.032	214	-0.15	GTF
05	40.8631	29.8100	0.699	0.048	34	not used	GTF
07	40.8750	29.9671	0.408	0.025	349	0.02	GTF
08	41.0369	30.0675	0.624	0.028	219	0.25	GTF
09	40.8319	30.1737	0.518	0.038	140	0.07	GTF
11	40.8535	31.5779	-0.129	0.039	31	-0.35	GTF
12	40.4877	29.0905	0.923	0.049	62	0.50	GTF
13	40.7232	29.5044	0.636	0.052	58	0.00	GTF
14	40.5673	29.5120	0.466	0.038	123	0.06	GTF
15	40.6827	29.9543	0.566	0.043	129	not used	GTF
16	40.5080	30.0187	0.708	0.030	196	0.28	GTF
18	40.6823	30.1988	0.298	0.035	128	-0.09	GTF
19	40.4717	30.2576	0.092	0.033	139	-0.44	GTF
20	40.5775	31.0112	0.646	0.030	108	0.23	GTF
24	40.6621	31.0411	0.092	0.041	37	not used	GTF
26	40.7253	31.3452	0.393	0.030	81	-0.03	GTF
27	40.6902	31.5733	0.811	0.038	45	0.41	GTF
28	40.9723	31.2089	0.501	0.074	26	0.28	SABO
29	40.6665	30.4315	0.577	0.031	147	0.32	SABO
30	40.7445	31.1771	0.302	0.027	164	-0.06	SABO
32	40.5579	30.8467	0.146	0.029	123	-0.38	SABO

Table 1 continue

ID	latitude	longitude	S	std	Nr	S_{B03}	Network
33	40.5440	31.0412	0.341	0.033	117	-0.03	SABO
34	40.6052	31.1453	0.217	0.028	171	-0.20	SABO
35	40.8214	30.8986	0.161	0.048	62	-0.21	SABO
36	40.9270	30.2065	0.414	0.064	25	not used	SABO
38	40.6006	30.6147	0.364	0.042	109	0.00	SABO
39	40.8978	30.6001	0	-------	242	-0.52	SABO
40	40.9573	30.3771	0.311	0.031	167	0.01	SABO
YPT	40.7639	29.7620	0.366	0.131	10	not used	KOERI
10_	40.7097	30.3953	0.110	0.168	15	not used	KOERI
14_	40.7496	30.5326	0.350	0.163	13	not used	KOERI
17_	40.7732	30.3978	0.508	0.171	9	not used	KOERI
09_	40.7624	30.3545	0.196	0.149	11	not used	KOERI
11_	40.7863	30.3907	0.407	0.174	10	not used	KOERI
15_	40.7369	30.3787	0.049	0.217	9	not used	KOERI
12_	40.7787	30.6785	-0.245	0.322	4	not used	KOERI
GEN	40.7849	30.3923	0.397	0.193	4	not used	KOERI
SEK	40.7847	30.3798	0.500	0.171	4	not used	KOERI
ARC	40.8236	29.3607	-0.142	0.273	9	not used	KOERI
DAR	40.7569	29.3673	0.023	0.277	12	not used	KOERI
HAS	40.8688	29.0875	-0.173	0.322	3	not used	KOERI
FAT	41.0197	28.9500	0.565	0.366	6	not used	KOERI
Has	40.6526	29.2631	0.031	0.335	5	not used	KOERI
Bag	40.6537	29.2743	0.049	0.316	8	not used	KOERI
Kas	40.6570	29.2915	-0.115	0.325	6	not used	KOERI
RAD	40.6504	29.3254	0.353	0.330	3	not used	KOERI
Ruz	40.6474	29.2768	0.161	0.312	8	not used	KOERI
GIR	40.6562	29.2956	0.081	0.363	4	not used	KOERI
Tar	40.6581	29.2476	0.044	0.360	7	not used	KOERI
Hil	40.6473	29.2645	0.021	0.350	6	not used	KOERI
Bah	40.6516	29.2824	-0.165	0.386	3	not used	KOERI

Stations used in this study. S and std are the average magnitude station correction and its standard deviation, respectively. Nr is the number of recordings used for the magnitude calibration. S_{B03} is the average magnitude correction found by Baumabach et al., 2003 (see their Table 2).

Figure captions

Figure 1. Analyzed data set. Top: SABO-GTF seismic (triangles) and KOERI strong motion (squares) stations. The identification number (staton ID) for the seismic stations (Table 1) are also shown. Station 39 is the reference station for the magnitude scale. The circles represent the locations of the considered earthquakes. Bottom: the black and gray lines are the path coverage for the seismic and strong motion neworks, respectivelty.

Figure 2. Resolution matrix: the logarithm of the values are shown. The parameter indexes within the ranges 1-61, 62-589, and 590-644 represent the attenuation coefficients, the magnitude values and the station corrections, respectively.

Figure 3. Unit covariance matrix: the logarithm of the values are shown.

Figure 4. Diagonal elements of the unit covariance matrix. a): values for the attenuation coefficients; b): values for the magnitudes of the earthquakes recorded by the GTF and SABO networks; c): values for the magnitudes of the earthquakes recorded by the KOERI network; d): values for the station corrections of the GTF and SABO networks; e): values for the station corrections of the KOERI network.

Figure 5. Results of the magnitude calibration. Top: comparison between the obtained LogAo function (vertical bars) and B03 (grey line). Middle: station correction ± one standard deviation. Bottom: magnitude values ± one standard deviation.

Figure 6. Top: magnitude versus distance. Middle: magnitude standard deviations versus the number of used recordings for each earthquake. Bottom: comparison between the magnitudes computed using the equation of B03 and of this study. The best fit in a least squares sense is also shown.

Figure 7. Magnitude residuals versus distance for the scale calibrated in this study (top) and by B03(bottom).

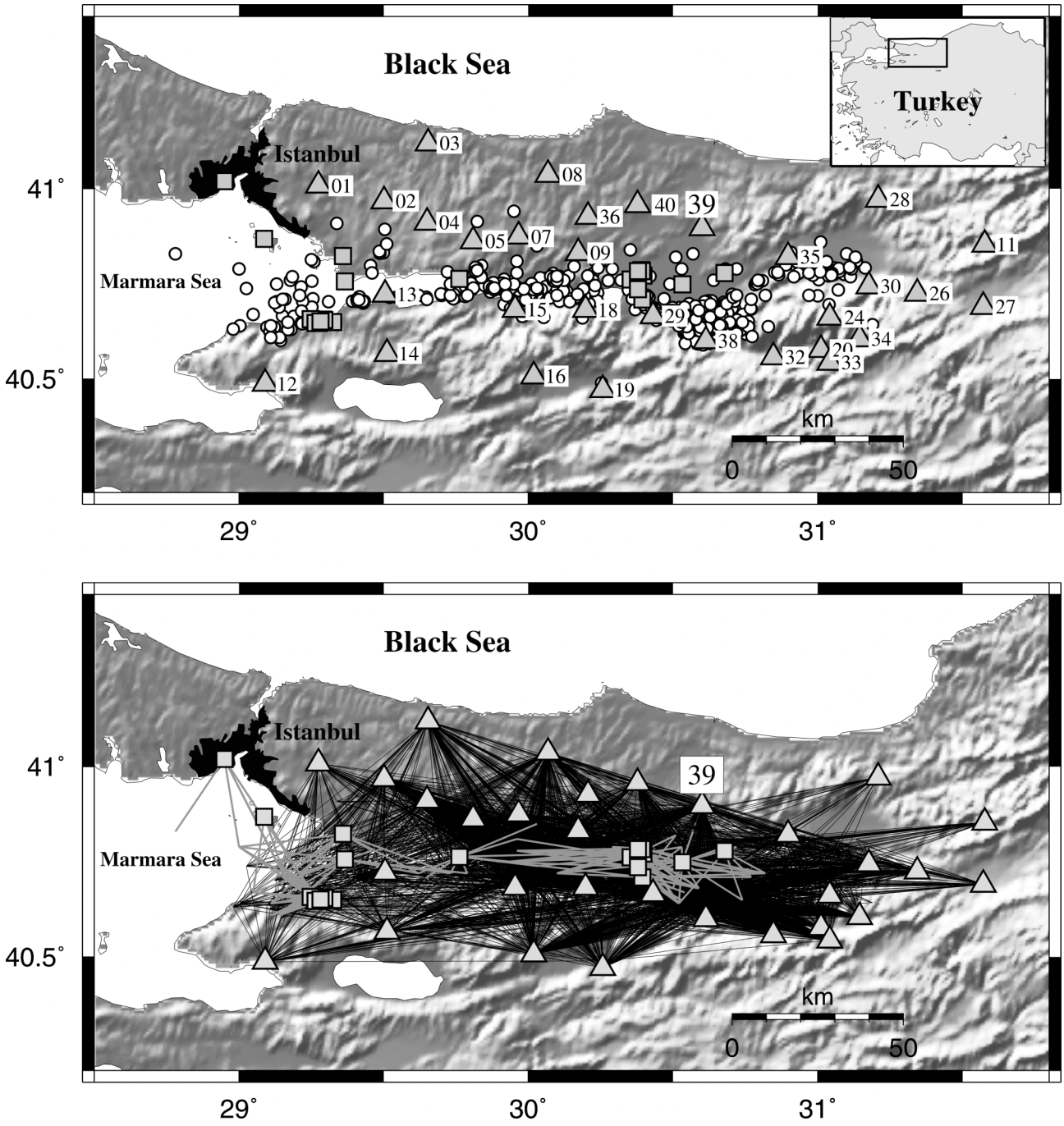
Black Sea
Turkey
Istanbul
Marmara Sea
41˚
40.5˚
29˚
30˚
31˚
km
0
50
01
02
03
04
05
07
08
09
11
12
13
14
15
16
18
19
20
24
26
27
28
29
30
32
33
34
35
36
38
39
40

Figure 1

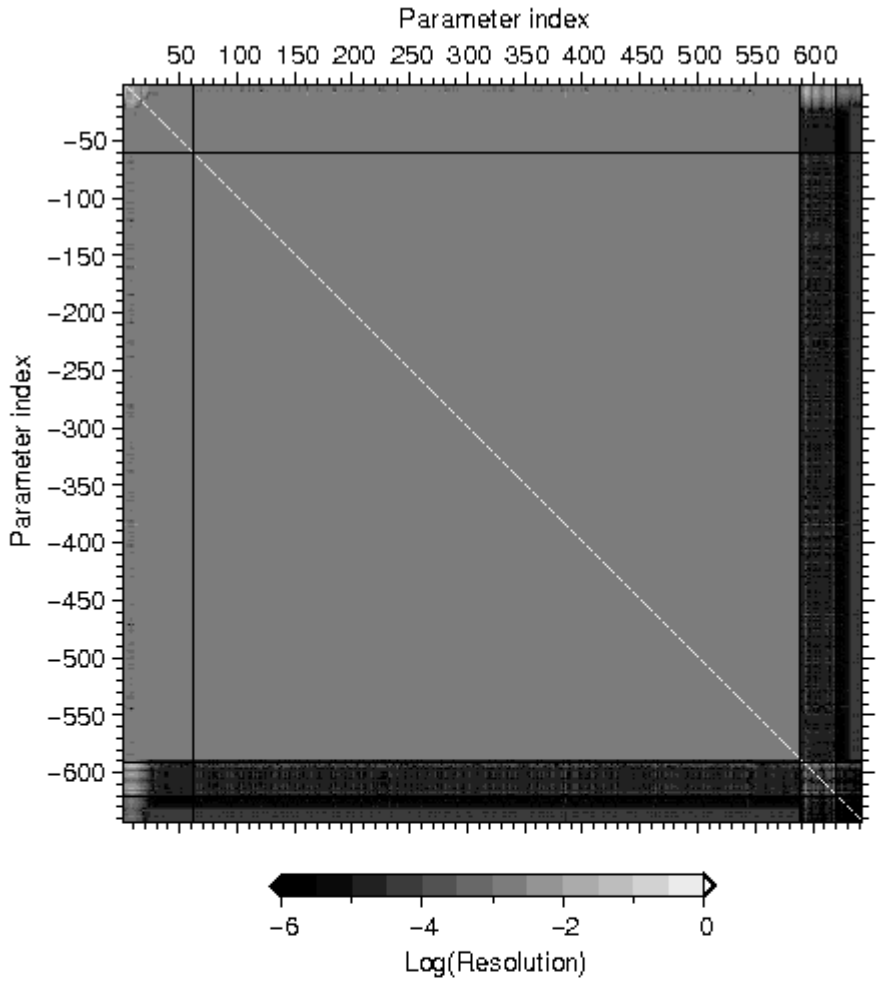
Parameter index
50 100 150 200 250 300 350 400 450 500 550 600
Parameter index
-50
-100
-150
-200
-250
-300
-350
-400
-450
-500
-550
-600
-6
-4
-2
0
Log(Resolution)

Figure 2

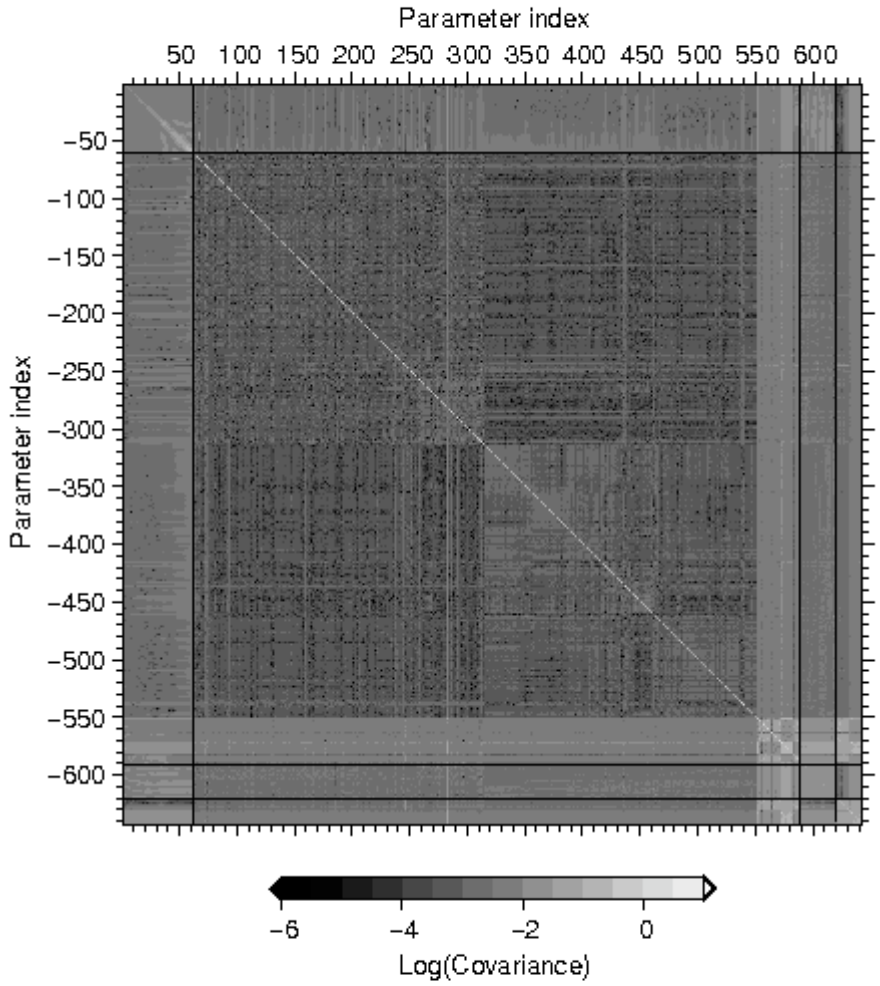
Parameter index
50 100 150 200 250 300 350 400 450 500 550 600
Parameter index
-50 -100 -150 -200 -250 -300 -350 -400 -450 -500 -550 -600
-6 -4 -2 0
Log(Covariance)

Figure 3

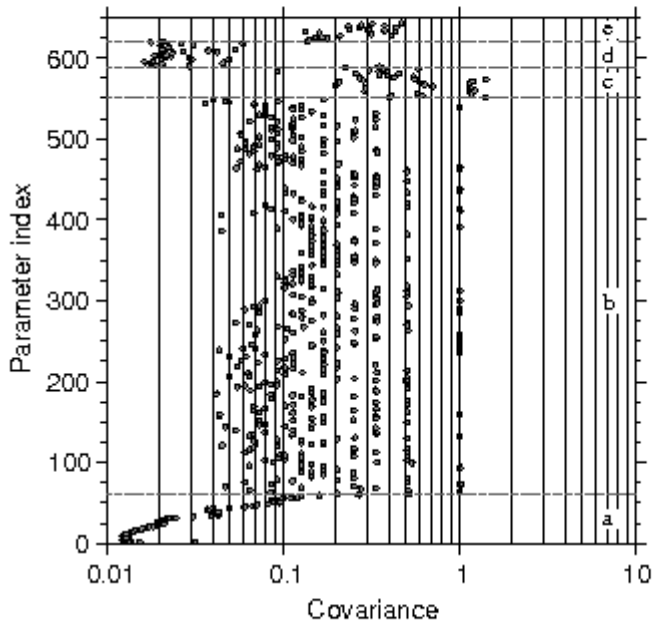
Parameter index
600
500
400
300
200
100
0
0.01
0.1
1
10
Covariance
e
d
c
b
a

Figure 4

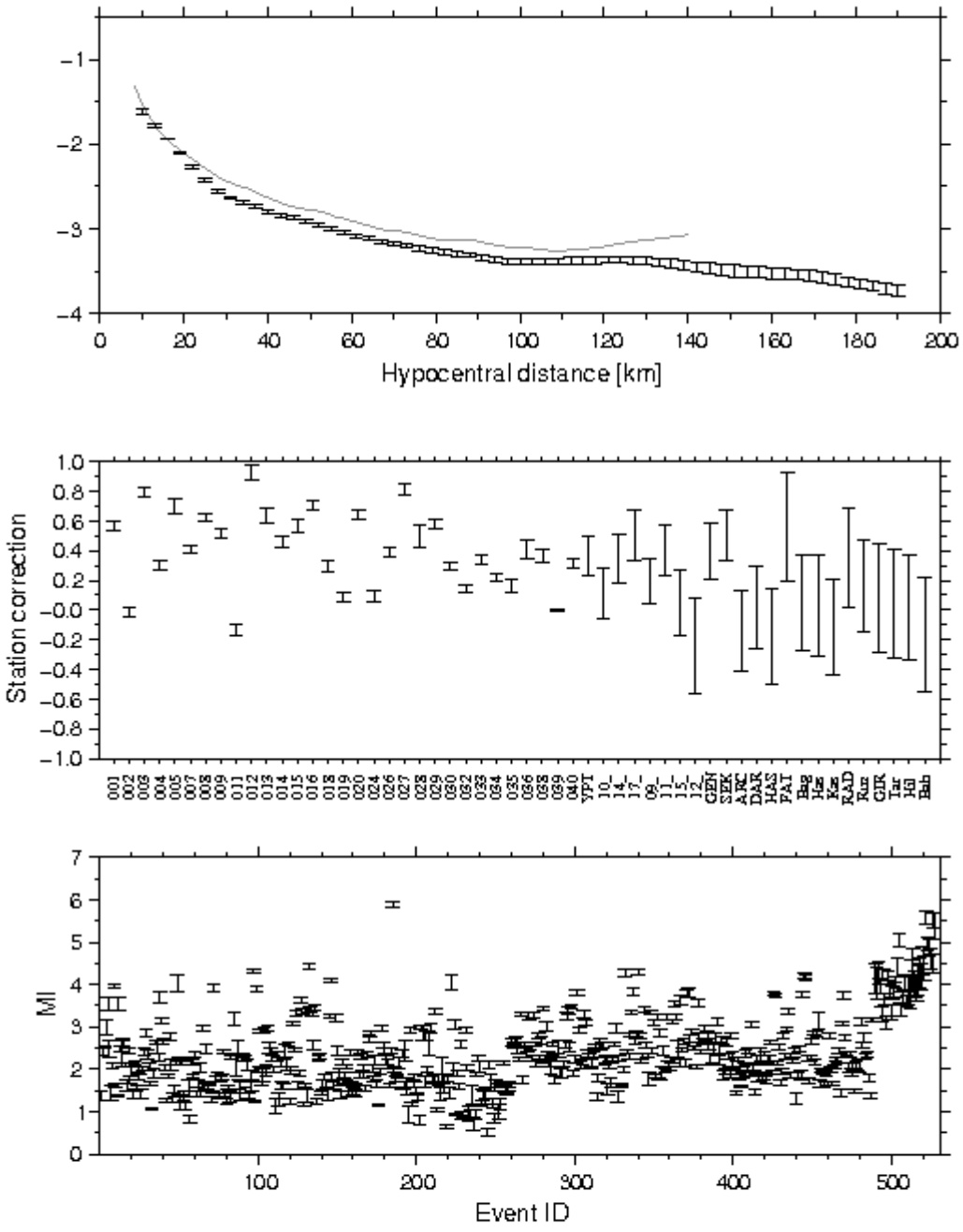

Figure 5

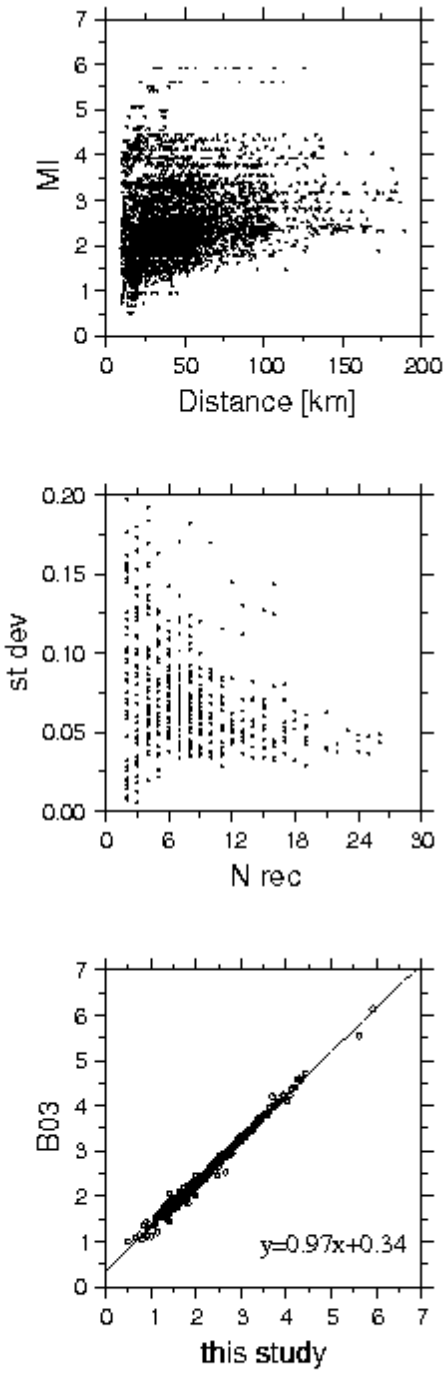

Figure 6

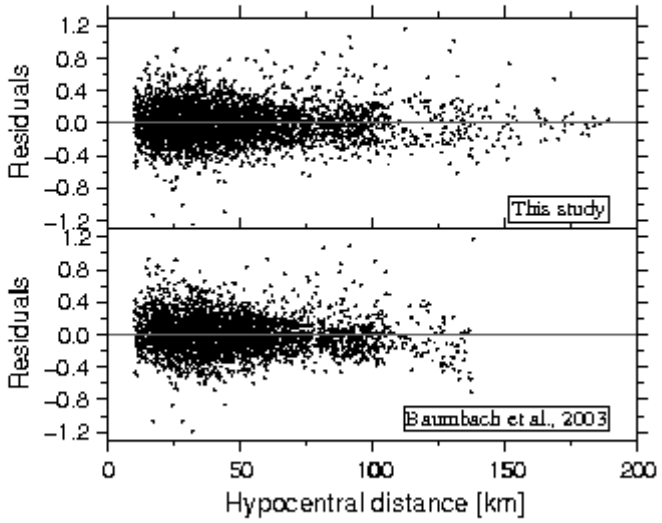
Residuals
1.2
0.8
0.4
0.0
−0.4
−0.8
−1.2
This study
Residuals
Baumbach et al., 2003
0
50
100
150
200
Hypocentral distance [km]

Figure 7